

Creating Three-Dimensional Models to Investigate Brittle Fracture in Polycrystalline Metals

G.E. Smith¹, A.G. Crocker¹, P.E.J. Flewitt^{2,3} and S Mahalingam²

Abstract: Three-dimensional models with irregular grain geometries and appropriate physical properties are needed to investigate fracture in polycrystalline metals and alloys. Creating such models is challenging but achievable using a two-stage process, suitable for any polycrystal. The processes described in this paper are illustrated by examples of brittle fracture in ferritic steel, zinc and nickel. The predicted crack path in a model is compared with the grain boundary fracture seen in three point bend specimens of nickel embrittled by sulphur.

Keywords: 3D models, polycrystalline metals, brittle fracture

1 Introduction

Two-dimensional (2D) modelling of crack propagation in polycrystals is inadequate because it fails to provide an adequate description of this 3D process. In the case of transgranular cleavage, 2D modelling does not consider the local accommodation required at a grain boundary as a crack passes from one grain to the next. Moreover, even for simple intergranular fracture, no consideration is given to the path at the tip of the crack. This becomes even more complex when, as is often the case, there is a combination of these two brittle failure mechanisms operating.

In general, the 2D models may be created by locating grain nuclei randomly in a plane and constructing Wigner-Seitz cells around them (Fig. 1).

In these models it is always possible for cleavage, represented by a line rather than a plane, to propagate across grain boundaries without any accommodating grain boundary failure, see Smith, G. E.; Crocker, A. G.; Moskovic, R.; Flewitt P. E. J. (2002). In practice, cleavage fracture planes on opposite sides of a boundary produce fracture traces in that boundary that do not coincide but reflect the different crystallographic orientations of the two parent grains, as shown schematically in

¹ Department of Physics, University of Surrey, Guildford, Surrey GU2 7XH, UK

² Interface Analysis Centre, University of Bristol, Bristol BS2 8BS, UK

³ School of Physics, University of Bristol, BS8 1TL, UK

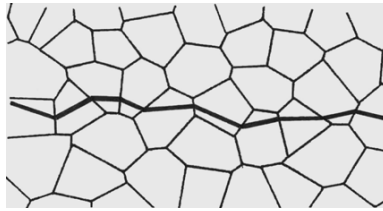


Figure 1: Example of a randomly generated 2D model polycrystal with a brittle crack.

Fig. 2. Some accommodating grain boundary failure or an equivalent mechanism must then occur if the material is to separate.

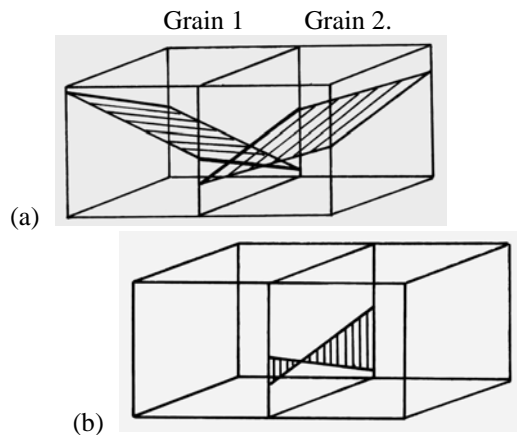


Figure 2: Grain boundary fracture is needed when a cleavage crack propagates from grain 1 across the grain boundary to grain 2.

For the simple case of two cubic grains, shown in Fig. 2, the shaded cleavage planes in (a) do not, in general, meet in a line in the grain boundary and the necessary accommodation is shown shaded in (b).

A very simple three-dimensional model of columnar prism grains which are encountered in a weld bead in a ferritic steel weldment, Fig. 3, shows the mismatches that can occur. This illustrates three different accommodation mechanisms in which cleavage cracks in adjacent grains (a) intersect, (b) meet at a grain edge and (c) do not meet. The area of grain boundary failure increases as the crack propagates outwards from the cleavage crack nucleated in the front grain, A.

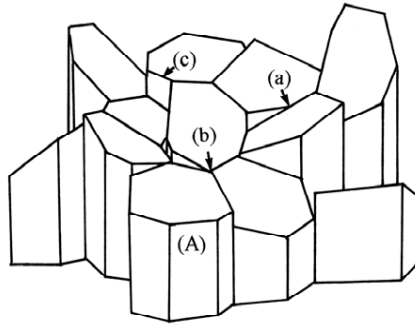


Figure 3: Part of a fracture surface of a model polycrystal consisting of columnar grains

To create realistic, if simplified, models of polycrystalline metals and validate them against experimental observations, it is important to develop efficient, versatile methods of creating and fracturing 3D models. It is also important to devise an economical data structure to hold the polycrystal connectivity and track the crack as it propagates so that larger models can be investigated. In this paper, we describe such a geometric model that allows both transgranular cleavage and intergranular brittle fracture to be modelled in polycrystalline materials with a defined crystal structure.

2 Model Polycrystal

2.1 Data structure

To hold structural information for each grain individually would be inefficient, as faces are shared by 2 grains, edges by 3 grains and vertices by 4 grains (Tab. 1). The solution adopted was to create a parent-child hierarchy for the grain components. Unique copies of faces, edges and vertices including parent-child information for each entry are held in a series of doubly-linked lists for each component type.

The number of children for a grain or a face is not known before the polycrystal is created. A schematic diagram shows the double linkages in Fig. 4.

The connections within a single tetrahedral grain are shown schematically in Fig. 5. The central black square represents the grain. Its four faces are shown as triangles; the next shell represents six edges and the outer corners the four vertices. All the faces, edges and vertices also have connections to surrounding grains (not shown).

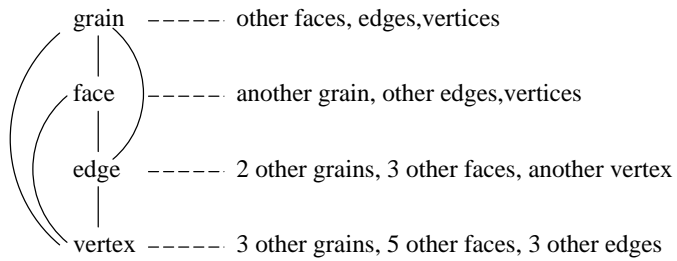


Figure 4: The parent child links between elements of the polycrystal

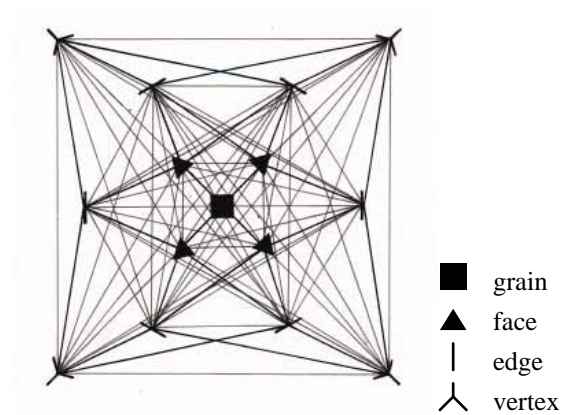


Figure 5: The parent-child links for a tetrahedral grain

Table 1: Relationships

component	parents	children
grain		faces edges vertices
face	2 grains	edges vertices
edge	3 grains 3 faces	2 vertices
vertex	4 grains 6 faces 4 edges	

2.2 Grain geometry

The geometry of the polycrystal may be generated separately from the crystallographic orientations of the grains or this may influence grain shapes. Constraints can be included in the software to ensure that grain shapes match those seen in the model material. For example some materials have elongated grains and others may have a bi-normal distribution of grain sizes. An example of columnar grains was shown in Fig. 3 and the later examples of ferritic steel and nickel have equi-axed grains.

A similar ethos to that for producing 2D Wigner-Seitz cells was adopted for the 3D models. Creating a model is a two stage process which generates two representations of the model space. The first is a voxel-based approximation of the grains. The second representation is the precise geometry of faces, edges and vertices. Initially, the co-ordinates for grain nuclei are randomly positioned within the model space. Special cases in which, for example, the grains are elongated or different grain sizes occur in different parts of the model can also be generated by constraining the distribution of the grain nuclei.

Model space is subdivided into a mesh of voxels, initially empty but gradually colonised by grains. This is achieved by allowing the grain nuclei to grow outwards in small steps, filling any unoccupied space until the whole of the model volume is filled with grains. From this mesh the co-ordinates of the vertices are calculated and from them the faces and edges of the 3D grains identified.

It is assumed that each vertex within the body of the model will have four parent grains. On the surface of the model space this reduces to three and on its edges to two. The first task is to find which grains share a common vertex. By stepping

through the model space with a small mask, it is possible to find all the small sub-volumes in which four grains meet. These volumes must each contain a single vertex shared by the four grains. The exact position of the vertex can be calculated from the co-ordinates of the nuclei of the four parent grains, as the vertex will lie at the centre of the unique sphere that passes through the four nuclei. If the nuclei have homogeneous co-ordinates $(x_i, y_i, z_i, 1)$ for $i= 1, 2, 3, 4$, the equation of the sphere that passes through them is given by the determinant below.

$$\begin{bmatrix} x^2 + y^2 + z^2 & x & y & z & 1 \\ x_1^2 + y_1^2 + z_1^2 & x_1 & y_1 & z_1 & 1 \\ x_2^2 + y_2^2 + z_2^2 & x_2 & y_2 & z_2 & 1 \\ x_3^2 + y_3^2 + z_3^2 & x_3 & y_3 & z_3 & 1 \\ x_4^2 + y_4^2 + z_4^2 & x_4 & y_4 & z_4 & 1 \end{bmatrix} = 0 \quad (1)$$

If the search of the model space finds a sub-volume where more than four grains meet, there would be more than one vertex within the sub-volume, indicating that the mesh was too coarse. The process is repeated with a finer mesh for this sub-volume.

In general, each vertex lies on the faces between pairs of its four parent grains. By selecting all vertices with two particular parent grains, all the vertices on the face between these two grains can be identified. If the grains grow at the same rate, these vertices must lie in the plane that is perpendicular to the line connecting the nuclei of the two grains and midway between them.

In the simplest cases, the grain boundaries (faces) are all randomly shaped polygons, as shown in Fig. 6. Here the grain boundaries are flat unlike those in real polycrystalline metals where the grains have curved faces that meet at defined angles. Some grain boundaries in the model are large; other boundaries are small; some have many edges, others as few as three.

Information about edge lengths, face areas and angles between edges can be extracted from the model, compared with experimental observation and used during the fracture simulation. Overall in the model illustrated there are many small faces and some faces are elongated. The angles at vertices range from 9° to 146° . The number of faces, edges and vertices for the five central grains (a-e) shown are given in Tab. 2 below.

All satisfy Euler's equation, $V-E+F = 2$ and can be compared with the results for the space-filling regular 14-hedron (tetrakaidecahedron) which has $F = 14$, $E = 36$, $V = 24$. Comparison with mean linear intercepts across grains, obtained experimentally, can be made most easily using the voxel representation. The distribution shown in Fig. 7 is for a model of 8,000 grains held in a $400 \times 400 \times 400$ mesh.



Figure 6: Five central grains shown linked together.

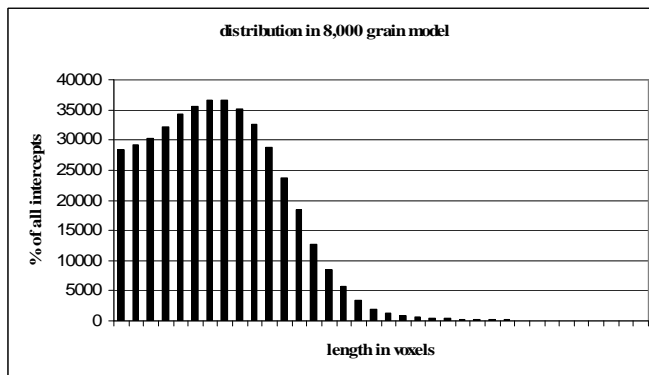


Figure 7: Distribution of linear intercepts

Table 2: Grain geometry

Grain	a	b	c	d	e	average
Faces (F)	14	15	15	13	14	14.2
Edges (E)	36	39	39	33	36	36.6
Vertices (V)	24	26	26	22	24	24.4

The more complex arrangement of grains with curved faces may be introduced by allowing grains to grow at different rates. Grain nucleation sites are again distributed randomly or constrained as before, but each is assigned a growth rate. A 2D slice through the model (Fig. 8) shows one black grain growing much faster than the white ones as they colonise the empty space. The white grains all have the same growth rate.

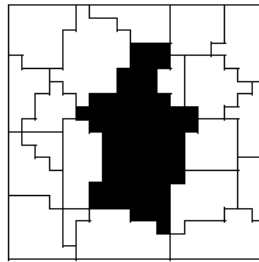


Figure 8: Black grain growing faster than the others (white)

The separation between two grain nuclei and the disparity in their rates of growth determine the position and curvature of their common face. For a growth ratio of g and separation d , the curved face is part of a sphere with centre at $d/(g^2-1)$ along the line connecting the two nuclei and radius $dg/(g^2-1)$.

Once the vertices of a face have been identified, the next step is to determine which pairs of these vertices are linked by edges. The vertices have been found by stepping through the model space and are not in a sequential order for the face (Fig. 9). They must be listed as children of the face in the correct order to link consecutive pairs as children of edges.

By choosing a suitable reference point, R in Fig. 10, the bearing of each vertex with respect to this point can be calculated, allowing the vertices to be ordered, when added to the face structure, as they would be found when traversing the perimeter of the grain boundary.

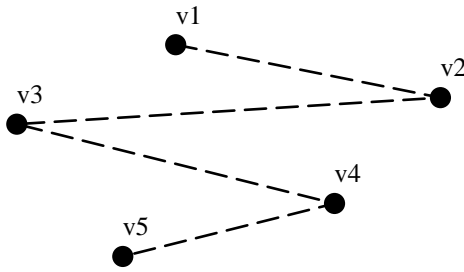


Figure 9: Possible vertex order initially

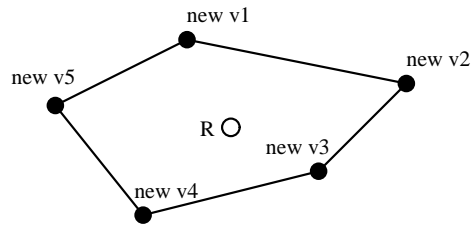


Figure 10: Vertices in sequential order

Grain edges are determined by taking successive pairs of vertices. This process is repeated for each pairing of parent grains that occurs. By adopting a protocol such as ordering parent grains by a reference index and selecting pairs in ascending sequence some duplication can be avoided. Each element identified is added to all the relevant parent-child lists. For example, when a new edge is found, its two end vertices are stored as its children and the edge is added to their parent list. In addition the edge is added as a child of its parent faces and grains and their child lists amended accordingly. At each stage any duplicates are discarded.

2.3 Physical properties

In general, the characteristics and history of the material determine the particular brittle fracture mode, either cleavage fracture or fracture along grain boundaries, see Argon, A.S.; Qiao, Y. (2002). This is achieved in the model by assigning relative fracture energies for each mode of failure appropriate for the temperature at which fracture is undertaken. Fracture along particular facets is governed by the orientation relative to the stress axis and additional factors explained later. The data structure developed for the polycrystal also includes the crystal structure, e.g. fcc, bcc or hcp, and thereby the transgranular cleavage planes etc. see Crocker, A. G.; Flewitt, P. E. J.; Smith, G. E. (2005).

The crystallographic orientation of each grain relative to a global co-ordinate system may be allocated randomly or constrained to mimic the observed orientations obtained from experimental observation. The number and relative orientations of possible cleavage and/or slip planes are determined by the model material. The orientations of these planes are expressed relative to their local grain co-ordinate system; they are then transformed to relate to the global co-ordinate system and stored in the data structure for each grain.

The relative energies of the boundaries are defined initially by the misorientation between the two adjacent grains. They are then modified by the presence of ei-

ther impurity or alloying element segregation at grain boundaries or prior damage. These energies are introduced as an additional factor modifying the fracture strength of each boundary individually.

Transgranular cleavage occurs on specific crystallographic planes related to the crystal structure of the material. Cleavage energy is the same for all cleavage planes but the resolved stress will be different depending on their global orientation. The fracture energies combined with resolved stress for two cleavage planes identically-oriented with respect to the stress axis in the model are assumed to be the same.

The strength of individual grain boundaries in the model, initially defined by the mismatch in orientation of their parent grains, is considered too complex to model directly at present and a simplification has been adopted. Values are assigned randomly from an appropriate distribution. If the thermo-mechanical history of the material has caused grain boundaries to become cavitated or decohered, this characteristic can be represented by including an appropriate multiplicative factor for each individual face either randomly or following some predetermined rule. Other factors, such as impurities or precipitation can also be included. The intrinsic strength and modifying factor for each grain boundary are held individually. This separation allows different simulations to change some of the physical properties independently while retaining the others unchanged.

3 Fracturing the model

A stress axis is chosen and fracture is initiated on the weakest and most highly stressed grain boundary or crystal plane. The resulting crack is then propagated across the model selecting the most vulnerable path at each stage. Depending on the material being modelled, its history and environmental conditions, there may be competition between several fracture modes, for example within the transition temperature range of the brittle to ductile transition range encountered in ferritic (bcc) steels. All relevant modes need to be included in the fracture simulation. Each mode is given an appropriate relative energy, which will be instrumental in determining the fracture mode selected at each decision point. In general, metals have several variants of the same crystallographic cleavage plane so that there is a higher probability of the crack tip, at a grain boundary, encountering a well-oriented cleavage plane in the grain ahead than the two grain boundary options. This leads to rougher fracture surfaces when failure is predominantly along grain boundaries than if the primary mode is cleavage fracture. However, cleavage fracture requires areas of accommodation fracture in grain boundaries in addition to the primary fracture.

The simulation identifies possible fracture events that could occur at a later time

ahead of the crack tip, selects the next event in the time-ordered list of possibilities, confirms this as occurring and removes any later events that are incompatible with the new event. The fracture path is held as a time-bonded list of fracture events. The list identifies fracture facets and their initiation times, together with the mode of fracture and area for each facet in a similar doubly-linked format to that of the polycrystal. The double linkage of the polycrystal structure allows the crack tip to be tracked from one grain to its outer faces and from these faces to their other parent grain. The fracture facets are linked in time order. As each new facet is found it is either inserted or appended to the sequence in the appropriate place. If a new fracture event identifies a grain for fracture that has already been added to the list at a later event time, this later event is removed.

As the crack tip reaches an unfractured grain, this grain failure and any it would initiate in unfractured neighbouring grains, are inserted into the time sequence fracture list. Although it is recognised that some grains or boundaries that are unfavourably oriented for fracture may be bypassed. These would separate eventually as the net section stress increases with the increase in the fracture surface area. The fracture simulation takes events in sequence from the time-ordered event list. If the next event in the list involves a grain that has already fractured, this event is discarded. The simulation continues until the crack has completely crossed the model. The facet areas for each fracture mode can be calculated by summing the areas in the fracture facet list and compared with experimental observations.

3.1 Cleavage fracture

In the case of metals with a bcc or hcp crystal structure such as ferritic steel or zinc respectively, if the grain boundaries are strong, the primary failure mode will be cleavage fracture in the brittle fracture temperature range. At low temperatures, cleavage fracture in low carbon ferritic steels or α -iron will occur on $\{100\}$ planes as measured in the grain co-ordinate system. Transforming these planes into the global co-ordinate system allows those best oriented, relative to the stress axis, to be identified. In general the modelling assumes that cleavage in a grain will initiate fracture in all unfractured neighbouring grains touched by that cleavage facet. This new fracture may be along the grain boundary or on the best oriented cleavage plane in the adjacent grain. Account has to be taken of relative fracture energies and orientations relative to the stress axis.

The fracture path is calculated based on two assumptions. The first is that cleavage fracture in a grain will be initiated from the first contact point with the crack tip and always selects the least resistant path forward. In 3D, the distance, p , of a point, (x', y', z') , from a plane with direction cosines l, m, n and passing through the point

(X, Y, Z) is given by Eq. 2 .

$$p^2 = \Sigma[m(z' - Z) - n(y' - Y)]^2 / (l^2 + m^2 + n^2) \quad (2)$$

The second assumption is that a second cleavage fracture will not be initiated in a grain that has already fractured. In deciding the fracture path in 3D, it is necessary to establish the first contact point of the crack tip with an unfractured grain. During a particular simulation, each fracture event has an associated time that records activation in the time sequence for the propagation of the crack. It is assumed that fracture along a cleavage plane will propagate radially when viewed as a projection in a plane perpendicular to the tensile stress axis. This corresponds to the crack spreading outwards elliptically along a planar cleavage face with the eccentricity determined by the angle of the plane to the stress axis. It is possible to create a time-bonded list of events by considering each initiating position on this projected plane for cleavage or grain boundary fracture in neighbouring grains and the distance of the initiating point from the precursor, as measured in the projected plane. In the example shown in Fig. 11, the stress axis is perpendicular to the projected cleavage facet and cleavage fracture has been initiated in a grain at the open circle at time, I_t . This is the first contact point between the crack tip and the grain, occurring at initiation time I_t in the simulation timeline. The crack propagates radially with the dotted arcs representing time steps. The black dots show the first grain boundary contact points as the cleavage fracture propagates into neighbouring grains A, B, C and D. This in turn initiates failure in grain A at time I_t+2 , in B at I_t+7 , in C at I_t+8 and in D at $I_t+9.5$ if they are unfractured. The data structure for each grain includes a flag indicating if it has fractured. If any of these grains are marked as fractured, no further propagation across those grains occurs. If the fracture of the cross-boundary grain impinges on the same boundary (not necessarily true) accommodation fracture of the boundary is required to link the facets. More complex connectivity, where the fracture in the cross-boundary grain does not reach this boundary, is seen as a second stage process.

The time values are calculated using geometry to find the shortest distance between a point and a line. (The words “side” and “corner” have been used to describe the two dimensional geometry in this analysis to avoid confusion with “edge” and “vertex” that are used for the three dimensional grain geometry.) In the projected 2D view of the cleavage facet, the first contact point of the facet with another grain would be at the intersection of the facet side with the perpendicular line that passes through the initiation point. If the intersection point lies within the side, propagation continues across a side. If the intersection point lies on an extension of the side, i.e. outside the side, propagation will be from a corner. For some configurations (A, B and C in this example) this intersection point lies outside the facet side and

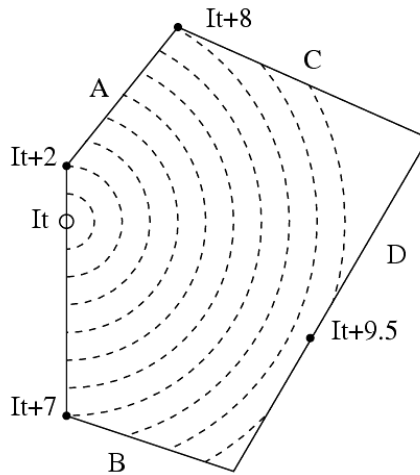


Figure 11: The projection of a cleavage facet on a plane perpendicular to the tensile stress axis.

propagation into these grains is from the corner of the facet. In the 3D model this corresponds to cleavage failure initiating at a grain face (as at D) or from a grain edge (A, B, C). Once the 2D coordinates of the new initiation points are known, the projection can be reversed to find the true 3D coordinates.

Although the primary fracture mechanism may be cleavage, some grain boundary fracture must also occur to connect the fracture planes if the model is to separate. Cleavage produces a multi-layered fracture surface. Fig. 12 shows the distribution

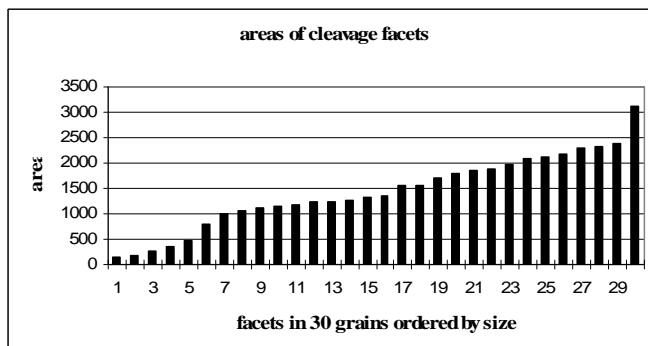
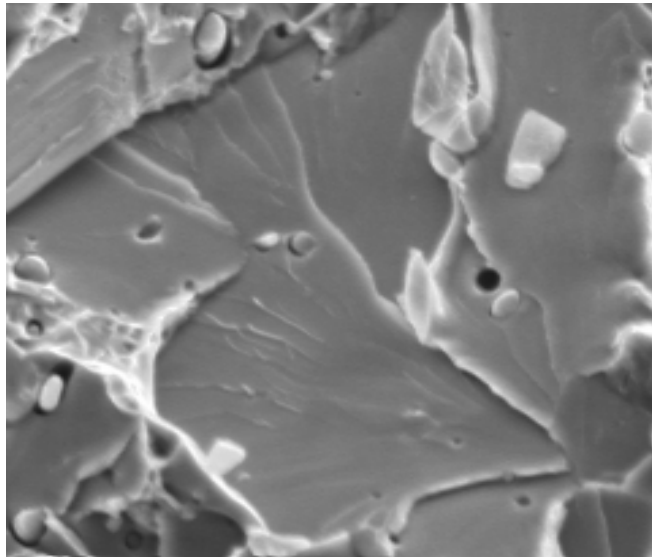


Figure 12: Distribution of 30 cleavage facet areas

of the areas of the cleavage fracture facets in 30 grains. The average cleavage facet area is 1,431 model units of area (mua) and the total is 42,916 (mua). This average size is approximately four times the size of the grain boundary facets plotted in Fig. 16. The model cross section is 10,000 mua. A scanning electron image of a typical (001) cleavage facet in an EN1A ferritic steel is shown in Fig. 18.



10 μm

Figure 13: Cleavage fracture in EN1A ferritic steel

Grain boundary accommodation adds approximately 7,330 mua to the total of 50,246 for all fracture facets. Most of the larger instances of accommodation fracture involve the larger grains but the moving average rises as the crack propagates farther from its initiation point. At a distance from the initiation point, it is quite common for the crack to propagate into two neighbouring grains independently and their fracture facets to involve the common boundary between the two grains creating fracture traces that have a large separation.

In some cases this potentially large accommodation fracture is reduced by stepped cleavage. This can be seen in the fracture surface of zinc (Fig.14), where two grains are separated by a boundary oriented diagonally across the picture. Planar cleavage fracture in the top grain has propagated into the lower grain with steps in the fracture surface of the lower grain to compensate for the mismatch in cleavage

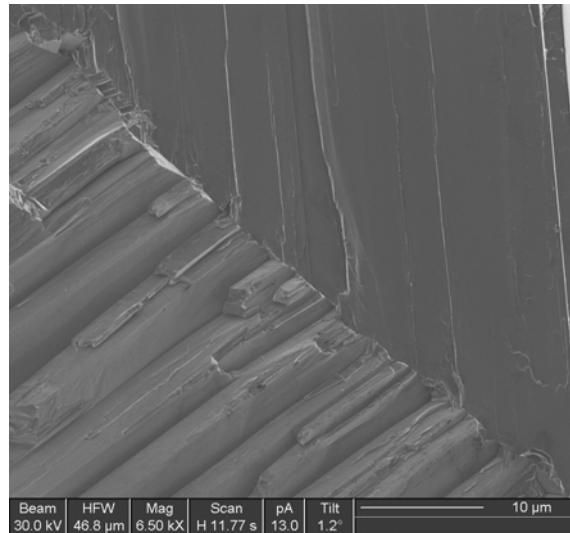


Figure 14: Stepped fracture in zinc

planes. See Hughes, G.M.; Smith, G.; Flewitt, P.E.J.; Crocker, A.G. (2007).

3.2 Grain boundary fracture

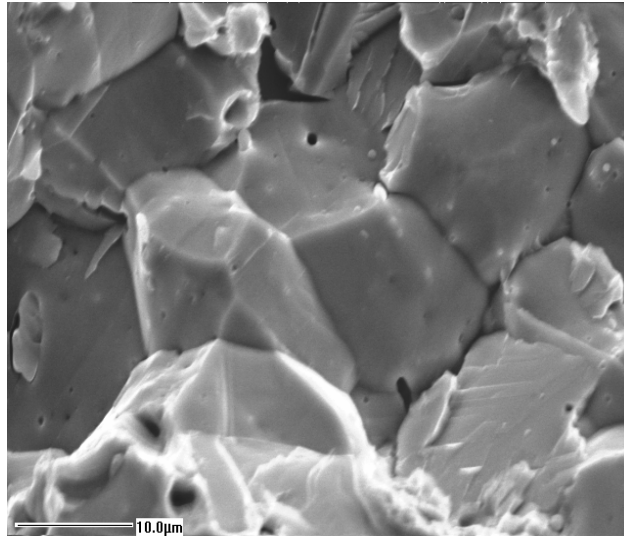
If grain boundaries are weak, the primary failure mode will be grain boundary fracture. An example is given in Fig. 15 of a scanning electron image for a thermo-mechanically treated EN1A ferritic steel.

A crack propagating along a grain boundary will reach the edges of that grain face. Each edge connects to two other grain faces allowing the fracture to continue along grain boundaries without the need for any secondary accommodation fracture. The orientations of the facets will have a wider distribution than if the cleavage fracture occurs. This leads to a rougher fracture surface. Li. M.; Xu, T. (2011)

In the distribution of grain boundary fracture facet areas, Fig. 16, the fracture surface has 40 facets with an average area of 332 model units of area (mua) and total area of 13,265 mua. This is for the same grain geometry as the previous example of cleavage failure (Fig. 12).

4 Nickel

Nickel is usually a ductile material but when it is embrittled by sulphur on the grain boundaries, intergranular fracture occurs for a range of temperatures. The chemical



10 μm

Figure 15: Intergranular fracture in EN1A ferritic steel

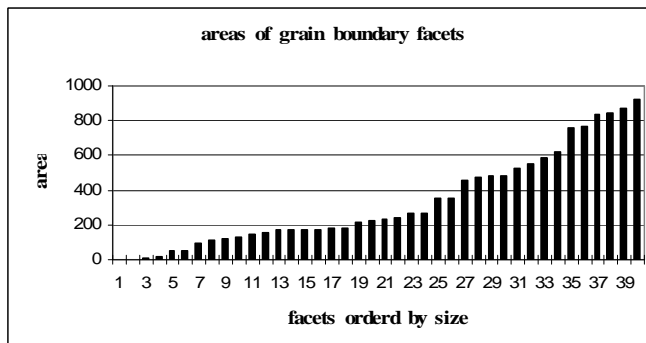


Figure 16: Distribution of grain boundary facet areas

composition by weight of the other elements present in the polycrystalline nickel is given in Tab. 3. The balance is nickel.

Table 3: Chemical composition (wt%)

Cu	Fe	Mn	Si	S	P	O
0.01	0.01	0.1	0.02	0.003	0.0004	0.043
Balance is nickel						

The solution was heat treated at 1017°C for 30 minutes, followed by air cooling, which resulted in a grain size of 200 μm. From this material three point bend geometry specimens with a notch ($a / w = 1/3$) were tested in the temperature range -196°C to 200°C. Brittle fracture was found to occur along weak grain boundaries up to temperatures of 150°C. The brittle to ductile transition graph is shown in Fig. 17. The left hand axis shows the fracture energy (Nmm) and the right hand axis the percentage of grain boundary fracture.

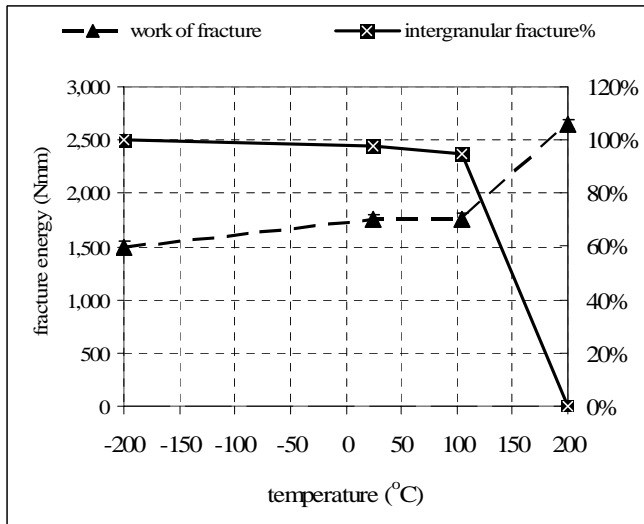


Figure 17: Brittle to ductile transition in nickel

The fracture surface, Fig. 18, consists of areas of grain boundary failure linked by ductile tearing. The dark areas indicate that some facets on the fracture surface are steeply inclined to the overall orientation of the surface. This characteristic is also seen in the model fracture surface, shown as a perspective projection in Fig.19.

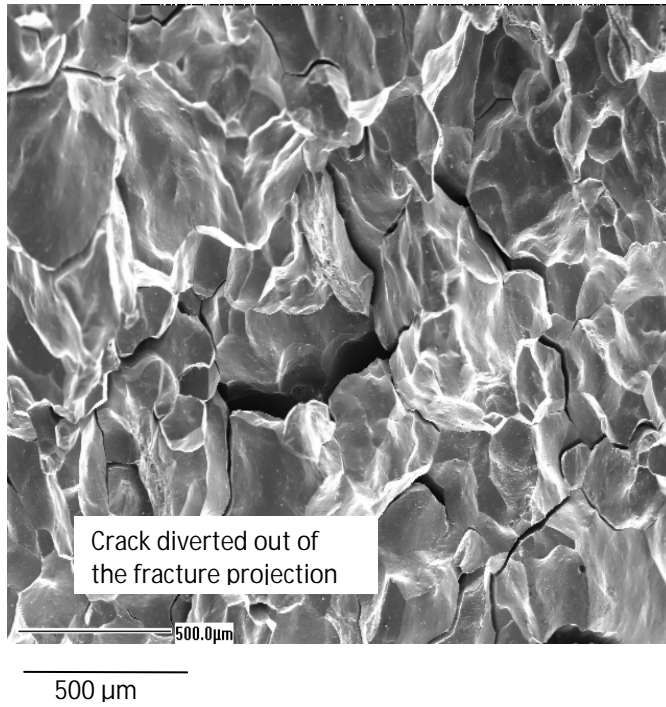


Figure 18: Scanning electron image of fracture surface in nickel at room temperature

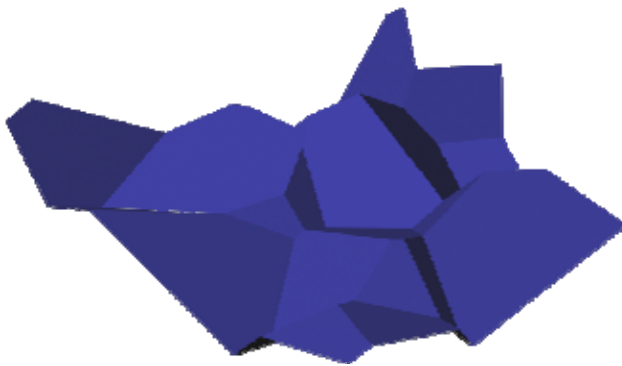


Figure 19: Model fracture surface in nickel

Conclusions

Models that simulate fracture have been developed over different length scales. Geometric models provide a bridge between Monte Carlo simulations and continuum mechanics based models. They provide information about areas and orientations of facets on a fracture surface that can be compared with what is observed experimentally in polycrystalline metals and alloys.

This paper provides the compelling reasons for developing 3D models to describe fracture in polycrystalline metals and alloys and some of the challenges associated with achieving this aim. There are many further refinements and extensions that could be added, such as twin boundaries or other sub-grain structure. Most of the diagrams and figures relate to a small model of 45 grains to illustrate issues simply but larger models have been created.

Acknowledgement: The authors would like to thank EPSRC for supporting this work (EP/H006729/1) and (EP/H007008/1). The research reported in this paper draws on the support, advice and findings of colleagues at other universities in the UK, in particular the research groups headed by Professor John Knott of Birmingham University and Professor Valerie Randle of the University of Wales, Swansea. It has been important to link this theoretical project with experimental observations to validate the models.

References

- Argon, A.S.; Qiao, Y.** (2002): Cleavage cracking resistance of large-angle grain boundaries in Fe-3 wt% Si alloy. *Philosophical Magazine a-Physics of Condensed Matter Structure Defects and Mechanical Properties*, 82, pp. 3333-3347.
- Crocker, A. G.; Flewitt, P. E. J.; Smith, G. E.** (2005): Computational Modelling of Fracture in Polycrystalline Materials, *Int. Materials Rev.*, 50(2), pp. 99-124.
- Hughes, G.M.; Smith, G.; Crocker, A.G.; Flewitt, P.E.J.** (2005): An examination of the linkage of cleavage cracks at grain boundaries. *Materials Science and Technology* 21, pp. 1268-1274.
- Hughes, G.M.; Smith, G. ; Flewitt, P.E.J.; Crocker, A.G.** (2007): *Proc. Roy. Soc. A*, 463, pp. 2129-2151
- Li, M.; Xu, T.** (2011): Topological and atomic scale characterization of grain boundary networks in polycrystalline and nanocrystalline materials, *Progress in Materials Science*, 56, pp. 864-899.
- Qiao, Y.; Argon, A. S.** (2003): Cleavage cracking resistance of high angle grain boundaries in Fe-3%Si alloy, *Mech. Mater.*, 35, 313-331.

Smith, G. E.; Crocker, A. G.; Moskovic, R.; Flewitt P. E. J. (2002): Models to describe brittle and ductile fracture in ferritic steels. *Philos. Mag.*, A82, 3443-3453.